Journal Name

ARTICLE TYPE

Cite this: DOI: 10.1039/xxxxxxxxxx

Alignment of ^{17}O-enriched water-endofullerene $H_2O@C_{60}$ in a liquid crystal matrix

Karel Kouřil,*[a] Benno Meier,[a] Shamim Alom,[a] Richard J. Whitby[a] and Malcolm H. Levitt*[a]

Received Date
Accepted Date

DOI: 10.1039/xxxxxxxxxx

www.rsc.org/journalname

We present a ^{17}O and ^{1}H NMR study of molecular endofullerene $H_2O@C_{60}$ dissolved in the nematic liquid crystal N-(4-methoxybenzylidene)-4-butylaniline (MBBA). The ^{17}O NMR peak is split into five components by the ^{17}O residual quadrupolar coupling, each of which is split into a triplet by the ^{1}H–^{17}O residual dipolar coupling and scalar coupling. The splittings are analysed in terms of the partial alignment of the encapsulated water molecules. Order parameters describing the alignment are estimated. It is found that the preferential orientation of the endohedral water molecule has the molecular plane perpendicular to the liquid crystal director.

1 Introduction

Molecular endofullerenes consist of closed carbon cages, such as C_{60}, each of which encapsulates a single small molecule, such as H_2, H_2O and HF[1–3]. The resulting complexes are denoted as $H_2@C_{60}$, $H_2O@C_{60}$ and $HF@C_{60}$. The endofullerenes may be prepared by molecular surgery techniques: chemically opening a fullerene cage, inserting a small molecule and closing the cage. Such techniques allow preparation of chemically pure endofullerenes in macroscopic quantities[3,4]. The pure endofullerenes are chemically stable black solids which can be readily investigated by a range of spectroscopic techniques such as nuclear magnetic resonance (NMR), inelastic neutron scattering (INS) and infrared spectroscopy (IR). Such investigations have shown that the encapsulated molecules have complete rotational freedom down to cryogenic temperatures and behave similarly to isolated gas molecules[3,5–9].

There are however differences between the encapsulated molecules and isolated free molecules – the encapsulated molecules show more complex behavior. Confinement in the cage leads to quantization of translational degrees of freedom and effects of rotation-translation coupling were observed under cryogenic conditions[5,6,8–10]. Furthermore some rotational levels of the guest molecules show reduced degeneracy in solid endofullerene samples. The most notable examples are $H_2@C_{60}$ and $H_2O@C_{60}$ which both show breaking of the triple degeneracy of their $J = 1$ states at cryogenic temperatures[7,11–13]. The lifting of degeneracy indicates reduction of symmetry of the environment in which the molecules are confined. This symmetry lowering has been interpreted in terms of fullerene cage distortion. Recently Felker and co-workers have shown that the interaction of the electric quadrupole moment of the confined molecule with the electrostatic potential of the adjacent C_{60} cages is sufficient to explain the observed splitting of the rotational levels even when the cages retain their icosahedral symmetry[14]. A symmetry reduction has also been observed at room temperatures by the solid-state NMR of $H_2O@C_{60}$[7,11] and $HF@C_{60}$[3].

Symmetry lowering in endofullerenes in anisotropic solvents was first observed by electron paramagnetic resonance (EPR) of the atomic endofullerenes $N@C_{60}$ and $N@C_{70}$ dissolved in the nematic liquid crystal N-(4-methoxybenzylidene)-4-butylaniline (MBBA)[15,16]. A NMR study of $H_2@C_{60}$, $H_2O@C_{60}$ and $HF@C_{60}$ in MBBA has shown clear signs of alignment of the encapsulated molecules[17]. In the anisotropic phase of the liquid crystal the ^{1}H lines of $H_2@C_{60}$ and $H_2O@C_{60}$ are split into doublets due to residual-dipolar-coupling (RDC) of the two ^{1}H nuclei. In the case of $HF@C_{60}$ both the ^{1}H and the ^{19}F spectra show an additional contribution to their doublet splitting from the RDC.

In case of diatomic endohedral molecules, a single RDC parameter is sufficient to describe the alignment of the molecule. However in the case of $H_2O@C_{60}$ this is not enough to fully characterize the alignment of the water molecule. Recently available ^{17}O-enriched $H_2O@C_{60}$ can provide more complete information on the behavior of the encapsulated water molecule. ^{17}O is a quadrupolar nucleus with spin-5/2. In isotropic solvents the ^{1}H and ^{17}O spectra show splittings (into sextet and triplet respectively) due to the J_{OH} scalar coupling[18]. The ^{1}H sextet peaks have non-equal widths due to the effect of scalar relaxation of the second kind, induced by coupling to the rapidly relaxing ^{17}O nucleus. Here we use the additional RDC as well as the residual quadrupolar coupling (RQC) to fully characterize the alignment of the endohedral water molecules in a solution of $H_2O@C_{60}$ in

[a] University of Southampton, Chemistry, SO17 1BJ, Southampton, United Kingdom
* E-mail: k.kouril@soton.ac.uk, mhl@soton.ac.uk

MBBA.

2 Experimental

$H_2{}^{17}O@C_{60}$ was prepared by means of molecular surgery[3,4] with 90% ^{17}O labeled water as starting material. Details of the synthesis are given in reference 18. The $H_2{}^{17}O@C_{60}$ powder was dissolved in MBBA using the same procedure as in reference 17. A small drop (volume $< 1\mu$l) of tetramethylsilane (TMS) was added to the solution to act as a chemical shift reference. This allows the observed shifts to be corrected for magnetic susceptibility changes (see below).

The NMR experiments were performed using a 500 MHz Bruker Avance III spectrometer with a standard 5 mm high-resolution probe. The ^{17}O spectra were measured using a pulse-acquire sequence. To suppress the broad background signal of the MBBA liquid crystal the ^1H spectra in the nematic phase were acquired using a perfect echo sequence[19–21]

$$90_x - \tau/2 - 180_y - \tau/2 - 90_y - \tau/2 - 180_x - \tau/2 - \text{acquire} \qquad (1)$$

with echo interval $\tau = 10$ ms. In the isotropic phase a pulse-acquire sequence was used to measure the ^1H spectra.

3 Results

3.1 ^{17}O NMR

A room temperature ^{17}O spectrum of $H_2{}^{17}O@C_{60}$ dissolved in nematic MBBA is shown in figure 1. The spectrum shows signs of residual quadrupolar coupling (RQC) and residual dipolar coupling (RDC). The ^{17}O nucleus has spin 5/2 as a result the RQC leads to splitting into a pentet. The lines are equidistant and the splitting is approximately 10520 Hz at $T = 298$ K. Each of the five lines arising from RQC is further split into 1:2:1 triplet. The splitting at 298 K is 208 Hz. The interactions responsible for this additional splitting are the scalar coupling $J_{OH} = -78$ Hz and the residual ^1H–^{17}O dipole – dipole interaction.

The lines in the triplet arising from the central transition of the ^{17}O nucleus are the sharpest in the spectrum with linewidth 19 Hz at $T = 300$ K. The lines corresponding to the first and second satellite transitions have linewidths 46 Hz and 96 Hz respectively.

Spectra observed at four different temperatures are shown in figure 2. When the temperature is increased the splittings (both pentet and triplet) decrease and the linewidths increase. On the nematic-to-isotropic phase transition of the liquid crystal solvent the pentet splitting induced by RQC vanishes. In the isotropic phase the spectrum consists only of a 1:2:1 triplet with a 78 Hz splitting due to ^1H – ^{17}O scalar coupling. This spectrum is consistent with the previously reported spectrum of $H_2{}^{17}O@C_{60}$ in isotropic solvents[18].

In order to extract temperature dependencies of the observed splittings the spectra recorded in nematic phase were fitted by a sum of five equidistant triplets composed of Lorentzian lines. All three lines in a given triplets had equal linewidths and fixed 1:2:1 amplitude ratio. Two parameters were used for the splittings, one for the pentet (RQC) splitting and one for the triplet splitting. The

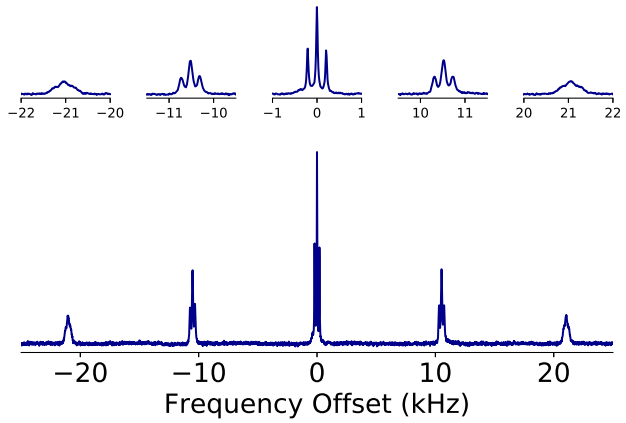

Fig. 1 A ^{17}O spectrum of $H_2{}^{17}O@C_{60}$ dissolved in MBBA. The spectrum was recorded at $T = 298$ K where the liquid crystal solvent is in the nematic phase. The ^{17}O line is split by residual quadrupole coupling into a pentet (approximately 10 kHz splitting). Details of the five lines are shown in the insets above the respective lines. Each of the five lines displays an additional smaller splitting into a 1:2:1 triplet (approximately 200 Hz). This smaller splitting is a combination of ^1H–^{17}O residual dipolar coupling and scalar coupling. The central line of the spectrum is at chemical shift -36 ppm.

following fitting function was used:

$$I(f) = \sum_{i=-2}^{2} \sum_{j=-1}^{1} \frac{1}{\pi(1+|j|)} \frac{A_{|i|} w_{|i|}}{(f - f_0 - i\Delta_P - j\Delta_T)^2 + w_{|i|}^2} \qquad (2)$$

The function has nine free parameters: center frequency f_0, pentet splitting Δ_P, triplet splitting Δ_T, three linewidths w_0, w_1, w_2 and three amplitudes A_0, A_1, A_2.

In the isotropic phase only a single triplet with 1:2:1 amplitude ratio was used to fit the spectra.

The temperature dependencies of the splittings are shown in figure 3. Both splittings show a gradual decrease with increasing temperature in the nematic phase and a discontinuity at the phase transition temperature. In the isotropic phase the pentet splitting vanishes while the triplet splitting is temperature independent and equal to the ^1H–^{17}O scalar coupling.

The temperature dependence of the ^{17}O chemical shift is shown in figure 4. This shift was corrected for magnetic susceptibility effects by using the ^1H TMS signal as a reference (see below). After the correction the ^{17}O chemical shift variability reduces to approximately 0.05 ppm throughout the $300 - 320$ K temperature range.

3.2 ^1H NMR

The ^1H spectra contain signals from the liquid crystal solvent, $H_2{}^{16}O@C_{60}$, $H_2{}^{17}O@C_{60}$ and TMS. The liquid crystal background consists of a broad unresolved signal in the nematic phase and narrow lines in the isotropic phase. The background and its suppression in the nematic phase were discussed previously[17].

The $H_2{}^{16}O@C_{60}$ spectra show the same behavior as reported previously[17]. In the nematic phase the spectrum consists of a doublet. On heating the splitting gradually reduces. In the

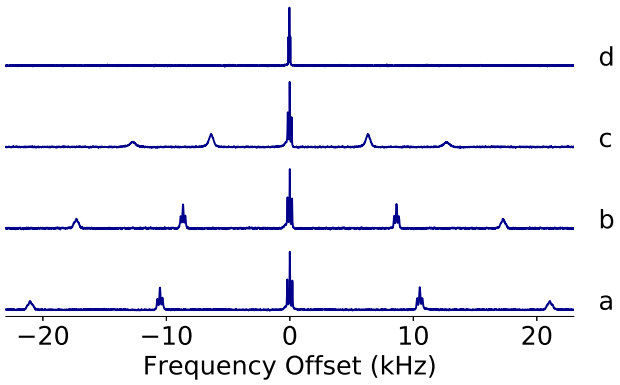

Fig. 2 ^{17}O spectra of $H_2{}^{17}O@C_{60}$ dissolved in MBBA at four different temperatures (a: T = 298 K, b: T = 303 K, c: T = 307 K, d: T = 315 K). Spectra a – c were recorded in the nematic phase. Spectrum d was recorded in the isotropic phase. In the nematic phase the spectrum shows signs of residual quadrupolar coupling and weaker residual dipolar coupling. Details of the nematic-phase spectrum are shown in figure 1. In the isotropic phase the spectrum consists of a 1:2:1 triplet showing a ^{1}H–^{17}O scalar coupling of $|J_{OH}| = 78$ Hz. The intensity of the spectrum d is scaled down by a factor of 10.

isotropic phase the spectrum consists of a single sharp line. The temperature dependence of the splitting is shown in figure 5.

In the nematic phase the ^{1}H spectrum of $H_2{}^{17}O@C_{60}$ could not be observed directly because of the strong background signal of the MBBA solvent. In the isotropic phase the spectrum consists of a sextet with splitting $|J_{OH}| = 78$ Hz. The ^{1}H spectrum of $H_2O@C_{60}$ in the isotropic phase is composed of the sextet from $H_2{}^{17}O@C_{60}$ and an additional sharp line from $H_2{}^{16}O@C_{60}$ [18].

The TMS ^{1}H spectrum consists of a single line in both the nematic and the isotropic phase of the liquid crystal solvent. No splitting due to RDC was observed which implies only very weak alignment of the molecule as expected from its high symmetry. The temperature-dependence of the TMS line frequency is attributed to a temperature-dependent magnetic susceptibility of the liquid crystal solvent. Such effects have been observed previously for ^{3}He dissolved in a liquid crystal [22].

The center frequency of the ^{1}H signal of $H_2{}^{16}O@C_{60}$ shows an analogous temperature dependence to that reported previously [17]. We used the temperature dependence of the TMS line frequency to subtract the susceptibility effect from the observed temperature dependencies of the ^{1}H and ^{17}O center frequencies. We estimate that residual chemical shift anisotropy (RCSA) contribution to the ^{1}H chemical shift of $H_2{}^{16}O@C_{60}$ at 300 K is approximately -0.1 ppm.

3.3 Correlation of observed splittings

Figure 6 shows the RDC splittings in the ^{1}H and the ^{17}O spectra plotted against ^{17}O RQC splitting for the same set of temperatures. The dependencies are fitted with linear functions and extrapolated to zero RQC splitting. The fit of the ^{1}H doublet splittings gave a slope 0.0589 ± 0.0004 and an intercept 6 ± 3 Hz. The fit of the ^{17}O triplet splittings gave a slope 0.0128 ± 0.0005 and

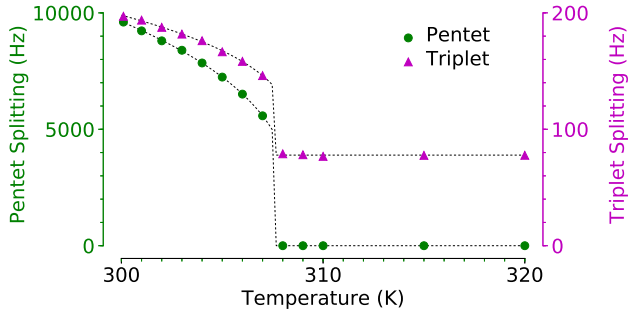

Fig. 3 Temperature dependencies of splittings observed in ^{17}O spectra. Green circles and left y-axis correspond to the pentet splitting while magenta triangles and right y-axis correspond to the triplet splitting. At lower temperatures, in the nematic phase, both splittings show gradual decrease on increasing temperature. At the nematic-to-isotropic phase transition there is a discontinuity in both splittings. Above the transition temperature, in the isotropic phase, the pentet splitting vanishes and the triplet splitting is constant and equal to the ^{1}H–^{17}O scalar coupling. The lines are fits to the Haller equation (see text and equation 3).

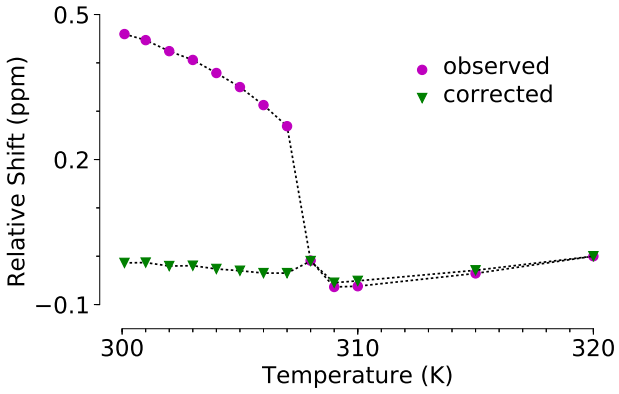

Fig. 4 Temperature dependence of the ^{17}O center line position of $H_2O@C_{60}$ in MBBA. Both the directly observed shift and the shift corrected for susceptibility effects (see text) are plotted. The shifts are plotted relative to the line position observed in isotropic phase at $T = 320$ K.

an intercept 75 ± 4 Hz. The intercept is positive and its magnitude is close to the ^{1}H–^{17}O scalar coupling. This indicates that the ^{1}H–^{17}O RDC has the same sign as the scalar coupling, i.e. it is negative [18].

4 Analysis

In an external magnetic field the director of the MBBA liquid crystal aligns parallel to the field. The order parameter of the liquid crystal is temperature dependent. The temperature dependencies of the splittings observed in the nematic phase can be fitted using the Haller equation [23] for the order parameter in the nematic phase

$$\Delta\omega(T) = \Delta\omega(0)\left(1 - \frac{T}{T^*}\right)^{\gamma}; \quad T \leq T_{NI} \tag{3}$$

where the nematic-to-isotropic phase transition temperature is denoted T_{NI}. For for $T > T_{NI}$ the splitting $\Delta\omega(T)$ either vanishes (^{17}O pentet and ^{1}H doublet) or becomes constant (^{17}O triplet).

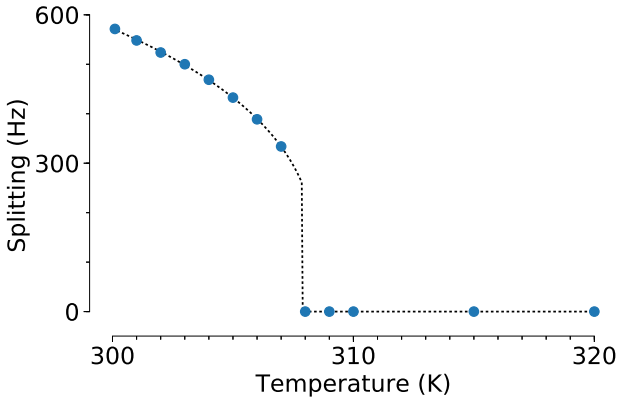

Fig. 5 Temperature dependence of the doublet splitting due to the ^{1}H–^{1}H residual dipolar coupling in $H_2{}^{16}O@C_{60}$. In the nematic phase the splitting decreases continuously with increasing temperature. At the nematic-to-isotropic phase transition the splitting vanishes. The line is a fit to the Haller equation (see text and equation 3).

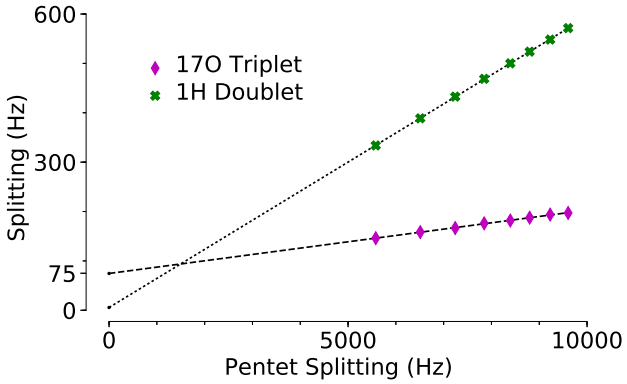

Fig. 6 Correlation of RDC related splittings and RQC pentet splitting observed in ^{17}O and ^{1}H spectra of $H_2O@C_{60}$ in the nematic phase of the liquid crystal solvent. The splittings show strong linear dependence on each other. The lines are linear fits to the data, extrapolated to zero RQC splitting. The intercept of the triplet splitting fit is 75 ± 4 Hz. Linear fit results are given in the text.

In general, the temperature origin T^* is slightly above T_{NI}. The fit results for the ^{17}O pentet are $\Delta\omega(0) = 2\pi$ 31 kHz, $T_{NI} = 307.6$ K, $T^* = 308.6$ K, $\gamma = 0.33$, for the ^{17}O triplet $\Delta\omega(0) = 2\pi$ 400 Hz, $T_{NI} = 307.5$ K, $T^* = 308.6$ K, $\gamma = 0.34$. For the ^{1}H doublet the fit gives $\Delta\omega(0) = 2\pi$ 1.8 kHz, $T_{NI} = 307.9$ K, $T^* = 308.6$ K, $\gamma = 0.32$. The transition temperatures T_{NI} are lower than those reported previously[17], this is attributed to the addition of TMS to the sample. The similar values of T^* and γ in all fits, together with the linear relations between all observed splittings (figure 6) indicate that the splittings are proportional to a common factor: the order parameter of the liquid crystal.

The NMR peak splittings in the nematic phase of a liquid crystal are due to the anisotropic nuclear spin interactions[24–28]. These interactions are averaged over rapid molecular motion. In an isotropic solvent these averages are zero. In the anisotropic phase the averaging yields small but non-zero values.

There are three types of relevant anisotropic interactions: (1) The electric quadrupole interaction of the ^{17}O nucleus with the electric field gradient generated by electrons surrounding the nucleus. The electric field gradient is fixed with respect to the water molecule. The motional average of this interaction is called the residual quadrupolar coupling (RQC)[29]. The RQC leads to a splitting of the ^{17}O line into five equidistant lines. (2) Magnetic through-space dipole-dipole interactions between the two ^{1}H nuclei in the H_2O molecule and between the ^{17}O and the ^{1}H nuclei. The motional average of these dipole-dipole coupling is called the residual dipolar coupling (RDC)[29–32]. The homonuclear ^{1}H–^{1}H RDC is responsible for the doublet splitting observed in the ^{1}H spectra of $H_2{}^{16}O@C_{60}$. In $H_2{}^{17}O@C_{60}$ the heteronuclear ^{1}H–^{17}O RDC combines with the ^{1}H–^{17}O J-coupling and contributes to the triplet splitting in the ^{17}O spectra. (3) The chemical shift anisotropy (CSA) which has a non-zero average value in an anisotropic solvent. This residual CSA (RCSA)[30,33] contributes to the chemical shift in the anisotropic phase.

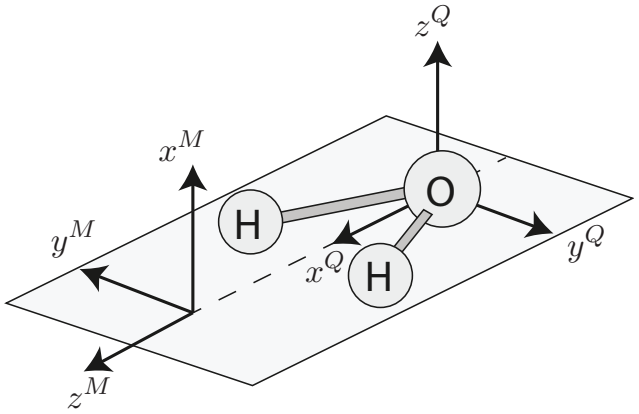

Fig. 7 Reference frames used for the treatment of anisotropic interactions in water. The molecular frame axes $\{x^M, y^M, z^M\}$ are aligned with the molecular symmetry axes as shown. The principal axes of the ^{17}O quadrupole coupling tensor are denoted $\{x^Q, y^Q, z^Q\}$, and are aligned as shown.

4.1 Averaging of the anisotropic interactions

We define the following reference frames: (1) A laboratory (lab) frame (L) with z-axis parallel to the applied magnetic field $\mathbf{B}_0$. (2) A molecular frame (M) which is fixed with respect to the encapsulated water molecule (see figure 7). The molecular plane is defined as the yz-plane, with the z-axis bisecting the H–O–H angle. The oxygen atom is at the origin, with the hydrogen atoms having positive z coordinates. This frame follows the random tumbling of the water molecule. (3) A set of principal axis frames (P^Λ) whose axes coincide with the principal axes of the spin interactions Λ. These frames have fixed orientations with respect to the molecular frame.

The relative orientation of two reference frames A and B is described by the Euler angles[34] $\Omega_{AB} = \{\alpha_{AB}, \beta_{AB}, \gamma_{AB}\}$. The frame A can be brought into coincidence with B by the following sequence of rotations: (1) Rotation by γ_{AB} around the z-axis of B, (2) rotation by β_{AB} around the y-axis of B, (3) rotation by α_{AB} around the z-axis of B.

Irreducible spherical tensors of rank λ may be transformed from frame A to B as follows[34]:

$$(F_{\lambda n})^{\mathrm{B}} = \sum_{m=-\lambda}^{\lambda} (F_{\lambda m})^{\mathrm{A}} D^{\lambda}_{mn}(\Omega_{\mathrm{AB}}) \tag{4}$$

where

$$D^{\lambda}_{mn}(\Omega_{\mathrm{AB}}) = \mathrm{e}^{-im\alpha_{\mathrm{AB}}} d^{\lambda}_{mn}(\beta_{\mathrm{AB}}) \mathrm{e}^{-in\gamma_{\mathrm{AB}}} \tag{5}$$

is the Wigner rotation matrix[34] of rank λ for Euler angles Ω_{AB} which bring the frame A into coincidence with the frame B. The term $d^{\lambda}_{mn}(\beta_{\mathrm{AB}})$ is the reduced Wigner rotation matrix of rank λ and β_{AB} is the angle between z axes of frames A and B.

In the secular approximation the Hamiltonian of an anisotropic spin interaction Λ can be written as following product of spatial and spin tensor components[26–28]:

$$H^{\Lambda} = \langle (A^{\Lambda}_{20})^{\mathrm{L}} \rangle T^{\Lambda}_{20} \tag{6}$$

where $(A^{\Lambda}_{20})^{\mathrm{L}}$ is the central element of the rank-2 irreducible spherical tensor describing the spatial part in the laboratory reference frame. The angle brackets denote averaging over the molecular motion. T^{Λ}_{20} is the central element of the rank-2 irreducible spherical tensor spin operator describing the interaction Λ.

The motionally-averaged central element of the spatial part of an interaction may be written as:

$$\langle (A^{\Lambda}_{20})^{\mathrm{L}} \rangle = \sum_{n=-2}^{+2} (A^{\Lambda}_{2n})^{\mathrm{M}} \langle D^{2}_{n0}(\Omega^{\Lambda}_{\mathrm{ML}}) \rangle \tag{7}$$

Where $(A^{\Lambda}_{2n})^{\mathrm{M}}$ are elements of the spherical tensor of interaction Λ in the molecular frame.

The five average elements of the Wigner rotation matrix $\langle D^{2}_{n0}(\Omega^{\Lambda}_{\mathrm{ML}}) \rangle$ are the five spherical order parameters of the H_2O molecule[26,27]:

$$S^2_n = \langle D^{2}_{n0}(\Omega^{\Lambda}_{\mathrm{ML}}) \rangle^* \tag{8}$$

$$S^2_n = (-1)^n (S^2_{-n})^* \tag{9}$$

The order parameters are the spherical components of the alignment tensor which describes the statistical properties of the water molecular orientation. From the symmetry of the water molecule, the principal axes of the alignment tensor coincide with the axes of the molecular frame. The alignment tensor is diagonal in the molecular frame so $S^2_{\pm 1} = 0$ and $S^2_{+2} = S^2_{-2}$ and only two order parameters are needed: S^2_0 and S^2_2.

The spatial parts of the anisotropic interactions are transformed from their respective principal axis frames into the (common) molecular frame as follows:

$$(A^{\Lambda}_{2n})^{\mathrm{M}} = \sum_{m=-2}^{+2} (A^{\Lambda}_{2m})^{\mathrm{P}} D^{2}_{mn}(\Omega^{\Lambda}_{\mathrm{PM}}) \tag{10}$$

4.2 ^{17}O quadrupolar coupling

The quadrupolar coupling constant C_{Q} is defined as:

$$C_{\mathrm{Q}} = \frac{e^2 q Q}{h} \tag{11}$$

where e is the elementary charge, eq is the largest eigenvalue of the electric field gradient tensor, Q is the nuclear quadrupole moment and h is the Planck constant.

The spatial part of the quadrupolar coupling expressed in the principal axis frame is given by[25–28]:

$$(A^{Q}_{20})^{\mathrm{P}} = \frac{\sqrt{6}\, 2\pi C_{\mathrm{Q}}}{4I(2I-1)} \tag{12}$$

$$(A^{Q}_{2\pm 1})^{\mathrm{P}} = 0 \tag{13}$$

$$(A^{Q}_{2\pm 2})^{\mathrm{P}} = \frac{2\pi C_{\mathrm{Q}} \eta_{\mathrm{Q}}}{4I(2I-1)} \tag{14}$$

where I is the nuclear spin ($I = 5/2$ for ^{17}O) and η_{Q} is the biaxiality of the electric field gradient tensor. The values of the coupling constants for the ^{17}O quadrupolar coupling in an isolated water molecule have been estimated by microwave spectroscopy in the gas phase[35] as $C_{\mathrm{Q}} = 10.169$ MHz and $\eta_{\mathrm{Q}} = 0.750$. The principal axis frame of the quadrupole interaction P^{Q} is oriented as shown in figure 7: The axis x^Q is parallel to the z axis of the molecular frame M, the axis y^Q is antiparallel to the y axis of M, and the axis z^Q axis is parallel to the x axis of M[35,36].

The spin part of the quadrupolar interaction is given by:

$$T^{\mathrm{Q}}_{20} = \frac{1}{\sqrt{6}} (3I^2_z - I(I+1)) \tag{15}$$

The RQC interaction leads to the splitting of ^{17}O resonance into five equidistant lines. The RQC splitting (the distance between adjacent lines of the pentet) can be written in terms of the order parameters and the spatial part of the quadrupole coupling (expressed in M frame) as follows[24]:

$$\Delta\omega^{\mathrm{RQC}}_{\mathrm{O}} = \sqrt{6} \left[(A^{Q}_{20})^{\mathrm{M}} S^2_0 + \left\{ (A^{Q}_{22})^{\mathrm{M}} + (A^{Q}_{2-2})^{\mathrm{M}} \right\} S^2_2 \right] \tag{16}$$

The relevant components of the spatial part of the quadrupolar interaction in the M frame are $(A^{\mathrm{Q}}_{20})^{\mathrm{M}} = -2\pi$ 77.8 kHz and $(A^{\mathrm{Q}}_{2\pm 2})^{\mathrm{M}} = 2\pi$ 477 kHz.

4.3 Dipolar couplings

The dipole-dipole coupling constant is defined as:

$$b_{12} = -\frac{\mu_0}{4\pi} \frac{\hbar \gamma_1 \gamma_2}{r^3_{12}} \tag{17}$$

where μ_0 is permeability of vacuum, $\hbar$ is the reduced Planck constant, γ_1, γ_2 are the gyromagnetic ratios of the two interacting nuclei and r_{12} is the internuclear distance.

For the two ^{1}H nuclei in the water molecule we get ($r_{\mathrm{HH}} =$ 152 pm) $b_{\mathrm{HH}} = -2\pi$ 34.5 kHz and for ^{1}H – ^{17}O we get ($r_{\mathrm{OH}} =$ 95.8 pm) $b_{\mathrm{OH}} = 2\pi$ 18.5 kHz.

In the principal axis frame the spatial part has only one non-zero component[26–28]:

$$(A^{12}_{20})^{\mathrm{P}} = \sqrt{6}\, b_{12} \tag{18}$$

$$(A^{12}_{2n})^{\mathrm{P}} = 0, \; n \neq 0 \tag{19}$$

The z axis of the principal axis frame lies parallel with the internuclear vector.

The central element of the spin part of the dipole-dipole interaction (expressed in the lab frame) is given by:

$$T_{20}^{\mathrm{dd}} = \frac{1}{\sqrt{6}}(3I_zS_z - \mathbf{I}\cdot\mathbf{S}) \tag{20}$$

where I_z and S_z are the z components of the two interacting nuclear spins $\mathbf{I}$ and $\mathbf{S}$.

The homonuclear ^{1}H–^{1}H RDC in $H_2{}^{16}O@C_{60}$ splits the ^{1}H signal into a doublet. The splitting can be expressed as[24]:

$$\Delta\omega_{\mathrm{HH}}^{\mathrm{RDC}} = \frac{3}{\sqrt{6}}\left[(A_{20}^{\mathrm{HH}})^{\mathrm{M}}S_0^2 + \left\{(A_{22}^{\mathrm{HH}})^{\mathrm{M}} + (A_{2-2}^{\mathrm{HH}})^{\mathrm{M}}\right\}S_2^2\right] \tag{21}$$

The values of the relevant components of the spatial part of the dipole-dipole interaction in the M frame are $(A_{20}^{\mathrm{HH}})^{\mathrm{M}} = 2\pi$ 42.3 kHz and $(A_{2\pm2}^{\mathrm{HH}})^{\mathrm{M}} = 2\pi$ 51.8 kHz.

In the heteronuclear ^{1}H–^{17}O case the effects of RDC were observed in ^{17}O spectra of $H_2{}^{17}O@C_{60}$ where they contribute to the observed triplet splitting:

$$\Delta\omega_{\mathrm{OH}}^{\mathrm{RDC}+J} = 2\pi J_{\mathrm{OH}} + \frac{2}{\sqrt{6}}\left[(A_{20}^{\mathrm{OH}})^{\mathrm{M}}S_0^2 + \left\{(A_{22}^{\mathrm{OH}})^{\mathrm{M}} + (A_{2-2}^{\mathrm{OH}})^{\mathrm{M}}\right\}S_2^2\right] \tag{22}$$

The values of the relevant components of the spatial part of the dipole-dipole interaction in the M frame are $(A_{20}^{\mathrm{OH}})^{\mathrm{M}} = 2\pi$ 2.82 kHz and $(A_{2\pm2}^{\mathrm{OH}})^{\mathrm{M}} = -2\pi$ 17.4 kHz. The scalar coupling is $J_{\mathrm{OH}} = -78$ Hz.

4.4 Chemical shift anisotropy

The spherical components of the spatial part of the chemical shift anisotropy are given by[26–28]:

$$(A_{20}^{\mathrm{CSA}})^{\mathrm{P}} = \sqrt{\frac{2}{3}}\Delta\sigma \tag{23}$$

$$(A_{2\pm1}^{\mathrm{CSA}})^{\mathrm{P}} = 0 \tag{24}$$

$$(A_{2\pm2}^{\mathrm{CSA}})^{\mathrm{P}} = \frac{1}{3}\Delta\sigma\eta \tag{25}$$

where $\Delta\sigma$ is the chemical shielding anisotropy and η is the biaxiality parameter.

The chemical shielding anisotropy in an isolated water molecule has been estimated as $\Delta\sigma^{\mathrm{H}} = 29$ ppm for the hydrogen nucleus[37] and $\Delta\sigma^{\mathrm{O}} = 47$ ppm for the ^{17}O nucleus[37]. The biaxiality parameters are nearly zero for both nuclei. The z axis of the P frame is along the O–H bond for the ^{1}H CSA. In case of the ^{17}O CSA the z axis of the P frame coincides with the z axis of the M frame.

The spin part is:

$$T_{20}^{\mathrm{CSA}} = \frac{1}{\sqrt{6}}2\gamma I_zB_0 \tag{26}$$

where γB_0 is the Larmor frequency and I_z is the operator of the z component of the nuclear spin.

The frequency shift due to the RCSA interaction is given by:

$$\Delta\sigma^{\mathrm{RCSA}} = \frac{2}{\sqrt{6}}\left[(A_{20}^{\mathrm{CSA}})^{\mathrm{M}}S_0^2 + \left\{(A_{22}^{\mathrm{CSA}})^{\mathrm{M}} + (A_{2-2}^{\mathrm{CSA}})^{\mathrm{M}}\right\}S_2^2\right] \tag{27}$$

The components of the ^{1}H CSA tensors in the M frame are $(A_{20}^{\mathrm{CSA:H}})^{\mathrm{M}} = 1.5$ ppm and $(A_{2\pm2}^{\mathrm{CSA:H}})^{\mathrm{M}} = -9.1$ ppm. The component of the ^{17}O CSA in the M frame are: $(A_{20}^{\mathrm{CSA:O}})^{\mathrm{M}} = 38$ ppm and $(A_{2\pm2}^{\mathrm{CSA:O}})^{\mathrm{M}} = 0$ ppm.

4.5 Order parameter estimates

The alignment of the encapsulated molecule is described by the two order parameters S_0^2 and S_2^2. At 300 K the observed splittings are: $|\Delta\omega_{\mathrm{O}}^{\mathrm{RQC}}| = 2\pi\times(9604\pm4)$ Hz, $|\Delta\omega_{\mathrm{HH}}^{\mathrm{RDC}}| = 2\pi\times(571\pm1)$ Hz and $\Delta\omega_{\mathrm{OH}}^{\mathrm{RDC}+J} = -2\pi\times(197\pm2)$ Hz. The signs of the RQC and ^{1}H–^{1}H RDC cannot be determined directly.

We used the expressions for the splittings (equations 16, 21, 22) given in the previous section to fit the order parameters to the experimental data. We assumed that the order parameters describing the alignment of the ^{17}O water molecule and the ^{16}O water molecule are the same. A good fit can only be obtained when the sign of the RQC splitting is assumed to be positive. An acceptable correspondence is obtained with either sign of the ^{1}H–^{1}H RDC. The resulting order parameters are $S_0^2 = (0.8\pm0.5)\times10^{-3}$ and $S_2^2 = (4.18\pm0.04)\times10^{-3}$ for positive ^{1}H–^{1}H RDC. For the negative ^{1}H–^{1}H RDC we get $S_0^2 = (-17.6\pm0.5)\times10^{-3}$ and $S_2^2 = (2.68\pm0.05)\ 10^{-3}$.

The order parameters were estimated using only the splittings induced by the RQC and the RDC interactions as these can be determined accurately from the observed spectra. The estimates of the RCSA have greater uncertainties but still can be used to decide between the two models. The ^{17}O RCSA at $T = 300$ K is nearly zero: $|\Delta\sigma_{\mathrm{O}}^{\mathrm{exp}}| < 0.05$ ppm and the ^{1}H RCSA is approximately $\Delta\sigma_{\mathrm{H}}^{\mathrm{exp}} \approx -0.1$ ppm. When we use the fitted order parameters to calculate the expected RCSA we get $\Delta\sigma_{\mathrm{H}}^{\mathrm{calc}} \approx -0.06$ ppm for both sets of order parameters, which is in reasonable agreement with the experiment. The ^{17}O RCSA however depends on the assumed sign of ^{1}H–^{1}H RDC. For the negative RDC we get $\Delta\sigma_{\mathrm{O}}^{\mathrm{calc}-} \approx -0.6$ ppm which is an order of magnitude larger than the experimental observation. For the positive RDC, on the other hand, we get $\Delta\sigma_{\mathrm{H}}^{\mathrm{calc}+} \approx 0.03$ ppm which agrees well with the experiment. We conclude that the following set of order parameters gives best agreement with experimental data at $T = 300$ K: $S_0^2 = (0.8\pm0.5)\times10^{-3}$ and $S_2^2 = (4.18\pm0.04)\times10^{-3}$. These order parameters correspond to positive ^{17}O RQC and positive ^{1}H–^{1}H RDC.

The two order parameters are components of the alignment tensor in spherical coordinates in the M frame. The cartesian components of the alignment tensor in the M frame are defined as[26,27]:

$$S_{ij} = \frac{1}{2}\left[3\langle\cos\alpha_i\cos\alpha_j\rangle - \delta_{ij}\right] \tag{28}$$

where α_i is the angle between the i axis of the M frame and the z axis of the L frame. The alignment tensor is diagonal in the M frame. Its diagonal components may be expressed in terms of the

order parameters as:

$$S_{xx} = \frac{1}{2}\left[\ \sqrt{6}\, S_2^2 - S_0^2\right] \quad (29)$$

$$S_{yy} = \frac{1}{2}\left[-\sqrt{6}\, S_2^2 - S_0^2\right] \quad (30)$$

$$S_{zz} = S_0^2 \quad (31)$$

The cartesian components of the alignment tensor are given in table 1. Their values indicate that the x axis of the M frame is preferentially parallel with the applied magnetic field (z axis of the L frame) and that the y axis of the M frame is preferentially perpendicular to it. The order parameter S_{zz} is approximately five times smaller than S_{xx} and S_{yy}: this indicates that there is little statistical preference for the H–O–H bisector to be either perpendicular or parallel to the liquid crystal director.

The favoured and disfavoured orientations of the water molecule relative to the liquid crystal director, as determined by this analysis, are sketched in figure 8.

Table 1 The cartesian components of the alignment tensor of the encapsulated water molecule. The components are given in the M frame where the tensor is diagonal.

Component	Value $\times 10^3$
S_{xx}	4.7 ± 0.3
S_{yy}	-5.5 ± 0.3
S_{zz}	0.8 ± 0.5

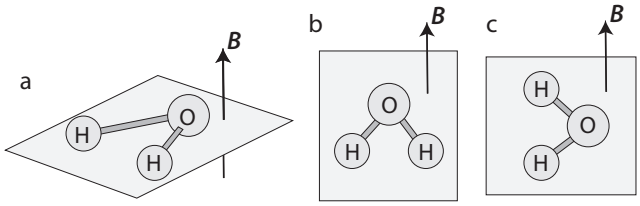

Fig. 8 Canonical orientations of the water molecule in $H_2{}^{17}O@C_{60}$ dissolved in MBBA, relative to the magnetic field B. Their representation in the ensemble, as deduced from the NMR data, is as follows. The orientation in (a), with the plane of the molecule perpendicular to the field, is slightly favoured in the ensemble ($S_{xx} = 4.7 \times 10^{-3}$); The orientation in (b), with the C_2 axis either parallel or antiparallel to the field, is also slightly favoured, but much less so than the orientation in (a) ($S_{zz} = 0.8 \times 10^{-3}$); The orientation in (c), with the H–H vector parallel to the field, is slightly disfavoured in the ensemble ($S_{yy} = -5.5 \times 10^{-3}$).

5 Conclusions

Analysis of the ^{17}O NMR spectra of $H_2{}^{17}O@C_{60}$ dissolved in the MBBA nematic liquid crystal allowed us to determine the alignment tensor of the encapsulated water molecule. Water orientations in which the H–O–H plane is perpendicular to the liquid crystal director (and the external magnetic field) are slightly favoured, water orientations in which the H-H internuclear vector is parallel to the liquid crystal director are slightly disfavoured.

There are two likely candidates for the mechanism of the observed alignment: (1) a direct mechanism in which the water molecule interacts directly with the field generated by the liquid crystal environment (through the walls of the C_{60} cage). A mechanism of this type has been used to explain symmetry breaking in solid endofullerenes[14]. (2) An indirect mechanism in which the C_{60} cages are assumed to acquire a geometrical or electronic distortion. The distorted cages are then aligned by the liquid crystal and in turn align the encapsulated water molecules.

We have not yet considered in detail whether the data described here may be used to distinguish between these two mechanisms. However, the cage distortion implied by the indirect mechanism may be expected to generate considerable chemical-shift anisotropy effects at the site of the water molecule. As described above, the CSA effects are found to be small, when confounding shifts due to susceptibility changes are accounted for. The absence of large CSA-related effects tends to favour the direct mechanism, in which the fullerene cages substantially retain their structural and electronic symmetry in the liquid crystal environment.

6 Acknowledgments

We acknowledge support from EPSRC (UK), grant numbers EP/M001962/1 and EP/P009980.

References

[1] K. Komatsu, M. Murata and Y. Murata, *Science*, 2005, **307**, 238–240.

[2] K. Kurotobi and Y. Murata, *Science*, 2011, **333**, 613–616.

[3] A. Krachmalnicoff, R. Bounds, S. Mamone, S. Alom, M. Concistrè, B. Meier, K. Kouřil, M. E. Light, M. R. Johnson, S. Rols, A. J. Horsewill, A. Shugai, U. Nagel, T. Rõõm, M. Carravetta, M. H. Levitt and R. J. Whitby, *Nature Chemistry*, 2016, **8**, 953–957.

[4] A. Krachmalnicoff, M. H. Levitt and R. J. Whitby, *Chem. Commun.*, 2014, **50**, 13037–13040.

[5] M. Xu, F. Sebastianelli, B. R. Gibbons, Z. Bacic, R. Lawler and N. J. Turro, *J. Chem. Phys.*, 2009, **130**, 224306.

[6] S. Mamone, M. Ge, D. Huvonen, U. Nagel, A. Danquigny, F. Cuda, M. C. Grossel, Y. Murata, K. Komatsu, M. H. Levitt, T. Rõõm and M. Carravetta, *J. Chem. Phys.*, 2009, **130**, 081103–4.

[7] C. Beduz, M. Carravetta, J. Y.-C. Chen, M. Concistrè, M. Denning, M. Frunzi, A. J. Horsewill, O. G. Johannessen, R. Lawler, X. Lei, M. H. Levitt, Y. Li, S. Mamone, Y. Murata, U. Nagel, T. Nishida, J. Ollivier, S. Rols, T. Rõõm, R. Sarkar, N. J. Turro and Y. Yang, *Proc. Natl. Acad. Sci. USA*, 2012, **109**, 12894–12898.

[8] M. H. Levitt, *Philos. T. Roy. Soc. A*, 2013, **371**, 20120429.

[9] S. Mamone, M. Jiménez-Ruiz, M. R. Johnson, S. Rols and A. J. Horsewill, *Phys. Chem. Chem. Phys.*, 2016, **18**, 29369–29380.

[10] A. J. Horsewill, S. Rols, M. R. Johnson, Y. Murata, M. Murata, K. Komatsu, M. Carravetta, S. Mamone, M. H. Levitt, J. Y. C. Chen, J. A. Johnson, X. Lei and N. J. Turro, *Phys. Rev. B*, 2010, **82**, 081410.

[11] M. Concistrè, S. Mamone, M. Denning, G. Pileio, X. Lei, Y. Li, M. Carravetta, N. J. Turro and M. H. Levitt, *Phil. Trans.*

R. Soc. A, 2013, **371**, 20120102.

[12] K. S. K. Goh, M. Jiménez-Ruiz, M. R. Johnson, S. Rols, J. Ollivier, M. S. Denning, S. Mamone, M. H. Levitt, X. Lei, Y. Li, N. J. Turro, Y. Murata and A. J. Horsewill, *Phys. Chem. Chem. Phys.*, 2014, **16**, 21330–21339.

[13] S. Mamone, M. R. Johnson, J. Ollivier, S. Rols, M. H. Levitt and A. J. Horsewill, *Phys. Chem. Chem. Phys.*, 2016, **18**, 1998–2005.

[14] P. M. Felker, V. Vlček, I. Hietanen, S. FitzGerald, D. Neuhauser and Z. Bačić, *Phys. Chem. Chem. Phys.*, 2017, **19**, 31274–31283.

[15] C. Meyer, W. Harneit, K. Lips, A. Weidinger, P. Jakes and K.-P. Dinse, *Phys. Rev. A*, 2002, **65**, 061201(R).

[16] G. Liu, M. d. C. Gimenez-Lopez, M. Jevric, A. N. Khlobystov, G. A. D. Briggs and K. Porfyrakis, *J. Phys. Chem. B*, 2013, **117**, 5925–5931.

[17] K. Kouřil, C. Wickens, B. Meier, S. Alom, J. GrÃďsvik, R. J. Whitby and M. H. Levitt, *Phys. Chemi. Chem. Phys.*, 2017, **19**, 11793–11801.

[18] S. J. Elliott, C. Bengs, K. Kouřil, B. Meier, S. Alom, R. J. Whitby and M. H. Levitt, *ChemPhysChem*, 2018, **19**, 251–255.

[19] K. Takegoshi, K. Ogura and K. Hikichi, *J. Magn. Reson.*, 1989, **84**, 611–615.

[20] J. A. Aguilar, M. Nilsson, G. Bodenhausen and G. A. Morris, *Chem. Commun.*, 2012, **48**, 811–813.

[21] G. Pileio, S. Bowen, C. Laustsen, M. C. D. Tayler, J. T. Hill-Cousins, L. J. Brown, R. C. D. Brown, J. H. Ardenkjaer-Larsen and M. H. Levitt, *J. Am. Chem. Soc.*, 2013, **135**, 5084–5088.

[22] R. Seydoux, O. Muenster and P. Diehl, *Molecular Crystals and Liquid Crystals Science and Technology. Section A. Molecular Crystals and Liquid Crystals*, 1994, **250**, 99–108.

[23] I. Haller, *Prog. Solid State Ch.*, 1975, **10**, 103–118.

[24] M. H. Levitt, *Spin Dynamics. Basics of Nuclear Magnetic Resonance*, Wiley, Chichester, 2nd edn, 2007.

[25] A. Jerschow, *Prog Nucl Magn Reson Spectrosc*, 2005, **46**, 63–78.

[26] J. W. Emsley, *Encyclopedia of Magnetic Resonance*, John Wiley & Sons, Ltd, Chichester, UK, 2007.

[27] J. Cavanagh, W. J. Fairbrother, A. G. Palmer III, M. Rance and N. J. Skelton, *Protein NMR Spectroscopy*, Academic Press, London, Second Edition edn, 2006.

[28] S. Chandra Shekar and A. Jerschow, *Encyclopedia of Magnetic Resonance*, John Wiley & Sons, Ltd, Chichester, UK, 2008.

[29] J. W. Emsley, G. R. Luckhurst and C. P. Stockley, *Proc. R Soc. Lond. A Math. Phys. Sci.*, 1982, **381**, 117–138.

[30] C. R. Sanders II, B. J. Hare, K. P. Howard and J. H. Prestegard, *Prog. Nucl. Magn. Reson. Spectrosc.*, 1994, **26, Part 5**, 421–444.

[31] N. Tjandra and A. Bax, *Science*, 1997, **278**, 1111.

[32] J. Prestegard, *Nature Struc. Bio.*, 1998, **5**, 492.

[33] G. Cornilescu, J. L. Marquardt, M. Ottiger and A. Bax, *J. Am. Chem. Soc.*, 1998, **120**, 6836–6837.

[34] D. A. Varshalovich, A. N. Moskalev and V. K. Kheronskii, *Quantum Theory of Angular Momentum*, World Scientific, Singapore, 1988.

[35] F. C. D. Lucia and P. Helminger, *J. Mol. Spectrosc.*, 1975, **56**, 138–145.

[36] O. V. Yazyev and L. Helm, *J. Chem. Phys.*, 2006, **125**, 054503.

[37] J. Vaara, J. Lounila, K. Ruud and T. Helgaker, *J. Chem. Phys.*, 1998, **109**, 8388–8397.